JBC RESEARCH ARTICLE

Mitochondrial membrane potential instability on reperfusion after ischemia does not depend on mitochondrial Ca^{2+} uptake

Received for publication, February 24, 2022, and in revised form, March 21, 2023 Published, Papers in Press, April 14, 2023,
https://doi.org/10.1016/j.jbc.2023.104708

Deepthi Ashok, Kyriakos Papanicolaou, Agnieszka Sidor, Michelle Wang, Soroosh Solhjoo, Ting Liu, and Brian O'Rourke*

From the Johns Hopkins University, Division of Cardiology, Department of Medicine, Baltimore, Maryland, USA

Reviewed by members of the JBC Editorial Board. Edited by Ruma Banerjee

Physiologic Ca^{2+} entry *via* the Mitochondrial Calcium Uniporter (MCU) participates in energetic adaption to workload but may also contribute to cell death during ischemia/reperfusion (I/R) injury. The MCU has been identified as the primary mode of Ca^{2+} import into mitochondria. Several groups have tested the hypothesis that Ca^{2+} import *via* MCU is detrimental during I/R injury using genetically-engineered mouse models, yet the results from these studies are inconclusive. Furthermore, mitochondria exhibit unstable or oscillatory membrane potentials ($\Delta\Psi_m$) when subjected to stress, such as during I/R, but it is unclear if the primary trigger is an excess influx of mitochondrial Ca^{2+} (mCa^{2+}), reactive oxygen species (ROS) accumulation, or other factors. Here, we critically examine whether MCU-mediated mitochondrial Ca^{2+} uptake during I/R is involved in $\Delta\Psi_m$ instability, or sustained mitochondrial depolarization, during reperfusion by acutely knocking out MCU in neonatal mouse ventricular myocyte (NMVM) monolayers subjected to simulated I/R. Unexpectedly, we find that MCU knockout does not significantly alter mCa^{2+} import during I/R, nor does it affect $\Delta\Psi_m$ recovery during reperfusion. In contrast, blocking the mitochondrial sodium-calcium exchanger (mNCE) suppressed the mCa^{2+} increase during Ischemia but did not affect $\Delta\Psi_m$ recovery or the frequency of $\Delta\Psi_m$ oscillations during reperfusion, indicating that mitochondrial $\Delta\Psi_m$ instability on reperfusion is not triggered by mCa^{2+}. Interestingly, inhibition of mitochondrial electron transport or supplementation with antioxidants stabilized I/R-induced $\Delta\Psi_m$ oscillations. The findings are consistent with mCa^{2+} overload being mediated by reverse-mode mNCE activity and supporting ROS-induced ROS release as the primary trigger of $\Delta\Psi_m$ instability during reperfusion injury.

Physiologic Ca^{2+} import into mitochondria is essential for matching energy supply with demand. Mitochondrial Ca^{2+} (mCa^{2+}) activates three Ca^{2+}-regulated dehydrogenases of the Krebs cycle (pyruvate dehydrogenase, 2-oxoglutarate dehydrogenase and isocitrate dehydrogenase) (1) and can regulate the activity of the ATP synthase (2) and cytochrome oxidase (3). Ca^{2+} overload is also a mainstay of current models of ischemia–reperfusion (I/R) injury. Excess mCa^{2+}, facilitated by an increase in reactive oxygen species(ROS), damages mitochondria and triggers cell death, principally through the opening of the mitochondrial permeability transition pore (mPTP), with the irreversible collapse of the mitochondrial inner membrane potential ($\Delta\Psi_m$) (4).

The mitochondrial calcium uniporter (MCU) has been identified as the primary mode of Ca^{2+} import into mitochondria (5–9) and several genetically-engineered mouse models have been used to test the hypothesis that MCU is detrimental during I/R injury. Surprisingly, mice with germline knockout of MCU did not show any protection from I/R injury (10). In addition, cardiac-specific overexpression of a dominant-negative MCU, which suppresses the activity of the endogenous channel, did not protect against I/R injury (11). In contrast, mice with inducible cardiomyocyte-specific deficiency of MCU (12, 13) or short-term inducible overexpression of MCUb (14) did protect against I/R injury. The discrepancies in outcomes have been attributed to possible adaptations of the organism to long-term inhibition of MCU that alter the mechanistic processes involved in myocyte damage (15).

Alternative explanations for the failure, in some cases, of MCU knockout to protect against I/R injury could be that (*i*) MCU may not be the only mode of Ca^{2+} entry into mitochondria during ischemia (16), or (*ii*) mitochondrial damage on reperfusion might occur through Ca^{2+}-independent mechanisms, such as through ROS-induced ROS release (RIRR) (17). With regard to the first point, a previous report suggested that the mCa^{2+} increase in cardiomyocytes during hypoxia is mediated by the reversal of the mitochondrial Na^+/Ca^{2+} exchanger (mNCE), and not by the MCU, based on its sensitivity to clonazepam but not ruthenium red (16). On the latter point, there is ample evidence that reversible $\Delta\Psi_m$ loss or oscillation can occur through ROS-dependent and Ca^{2+}-independent mechanisms during metabolic or oxidative stress. For example, our group has shown that oscillations of $\Delta\Psi_m$ and redox potential can be triggered in local clusters of mitochondria, or synchronize across the entire mitochondrial network of a cardiomyocyte (18, 19), in response to various

Lead contact: Further information and requests for resources and reagents should be directed to and will be fulfilled by the lead contact, Brian O'Rourke (bor@jhmi.edu).
* For correspondence: Brian O'Rourke, bor@jhmi.edu.

methods to induce oxidative stress (20), even when cellular Ca^{2+} is depleted. Similarly, single mitochondrion superoxide "mitoflashes" (21), redox/pH transients (22), or local RIRR events induced by a laser (17), may be modulated by, but are not obligatorily dependent on, Ca^{2+}. This leaves open the possibility that mitochondrial $\Delta\Psi_m$ instability and cellular damage could be primarily driven by ROS rather than mCa^{2+}, at least during early reperfusion.

The post-ischemic heart is also prone to ventricular arrhythmias that have been linked to RIRR-triggered $\Delta\Psi_m$ instability but were not sensitive to the mPTP inhibitor cyclosporine A (23, 24). Treatment with ligands of the mitochondrial benzodiazepine receptor prevented ventricular arrhythmias on reperfusion (23) and stabilized $\Delta\Psi_m$ oscillations (25), potentially implicating Inner Membrane Anion Channels (26) or the outer membrane Translocator Protein (27) in this process (28). These data support the possibility that alternative, mPTP-independent, mitochondrial targets may contribute to $\Delta\Psi_m$ instability and electrophysiological abnormalities during reperfusion.

Here, we critically examine whether MCU-mediated mitochondrial Ca^{2+} uptake during I/R is involved in triggering $\Delta\Psi$m oscillations or sustained mitochondrial depolarization during reperfusion. Employing acute knockout of MCU in a cellular model of I/R in neonatal mouse ventricular myocytes, we show that MCU deficiency has no effect on $\Delta\Psi_m$ recovery or oscillation on reperfusion. Moreover, MCU knockout did not affect mCa^{2+} import during I/R, while inhibition of the mitochondrial Na^+/Ca^{2+} exchanger (mNCE) did, challenging the paradigm that MCU is the primary mode of mCa^{2+} import during ischemia.

Results

MCU is required for rapid Ca^{2+} uptake into mitochondria during excitation–contraction coupling

Ca^{2+} uptake into the mitochondria is driven by the electrochemical Ca^{2+} gradient and the negative membrane potential inside mitochondria (29, 30). MCU is the primary mode of Ca^{2+} entry into the mitochondria and is responsible for the rapid uptake of mCa^{2+} (5, 8, 30). Because we were interested in the functional effects of acute knockout of the MCU gene, while minimizing potential systemic adaptative responses, we utilized a viral gene transfer method to express Cre recombinase to achieve MCU knockout (∼80% decrease) within 5 days in culture (Fig. 1, *C* and *D*). We first measured mCa^{2+} levels in neonatal mouse ventricular myocytes (NMVMs) using the genetically encoded MitoCam (4mtd3cpv) FRET probe (Fig. 2*A*). We recorded baseline mCa^{2+} levels in unstimulated cells for 10 min, acquiring an image every 15 s. We found no difference between matrix resting Ca^{2+} levels in MCU-WT and KO cells, similar to observations in several other MCU knockout studies (12, 13, 31). Blocking the mitochondrial Na^+/Ca^{2+} exchanger with the mNCE inhibitor CGP-37157 (CGP;10 μM) also did not alter baseline mCa^{2+} levels (Fig. 2*A*). However, when we measured beat-to-beat mCa^{2+} transient amplitudes in MCU-WT and MCU-KO myocytes (Example traces in Fig. S1), we observed a 55% decrease in MCU-KO myocytes compared to WT (Fig. 2*B*). To determine if there was any difference in mCa^{2+} uptake in response to a large rise in cytosolic Ca^{2+}, we initiated caffeine-induced SR-Ca^{2+} release (32). Cells were superfused with Na^+- and Ca^{2+}-free buffer to prevent Ca^{2+} extrusion *via* the sarcolemmal Na^+/Ca^{2+} exchanger (NCX). Then 20 mM Caffeine was then added to release the SR-Ca^{2+} stores. Under these conditions, Ca^{2+} accumulation in the mitochondria was measured. We found that mCa^{2+} uptake into the mitochondria was significantly reduced by ∼80% in MCU-KO cells (Fig. 2*C*). Calibration of the MitoCam probe in both WT and KO cells to obtain the minimum (R_{min}) and maximum (R_{max}) YFP/CFP FRET ratios showed no differences in R_{min} and R_{max} between MCU-WT and KO cells (Fig. 2, *D* and *E*). Examples of the calibration traces are shown in Fig. S2. Further, since the mitochondria contribute to beat-to-beat buffering of systolic Ca^{2+} transients (33) *via* MCU, we also measured cytosolic Ca^{2+} transients using Fura-2. MCU-KO monolayers displayed a ∼37% increase in cytosolic Ca^{2+} transient amplitude compared to WT. Adding 10 μM CGP to WT cells increased cytosolic transient amplitude by ∼24% compared to controls (Fig. 2*F*). While it is presently unclear why we observe this increase, this demonstrates that CGP does not inhibit cytosolic Ca^{2+} cycling (important for the subsequent interpretation of its effect on I/R Ca^{2+}). These results show that, although there is no difference in matrix Ca^{2+} levels at baseline between MCU-WT and KO, fast mCa^{2+} uptake is significantly reduced in MCU-KO cells.

MCU knockout does not affect mitochondrial Ca^{2+} import during ischemia and reperfusion, but inhibiting mNCE prevents mCa^{2+} increase during ischemia

Excessive Ca^{2+} influx into mitochondria during metabolic stress can trigger cell death pathways *via* mPTP (34), leading to the hypothesis that preventing or reducing Ca^{2+} influx into mitochondria during ischemia could be beneficial. Nevertheless, there have been conflicting reports of the role of MCU on *in vivo* I/R injury (10–13), so we next assessed the impact of genetic knockout of MCU on mitochondrial Ca^{2+} uptake during I/R injury. Particularly, we wanted to understand the mechanisms of Ca^{2+} import into mitochondria during I/R while simultaneously monitoring $\Delta\Psi_m$. To monitor mitochondrial Ca^{2+}, an adenovirus expressing MitoCam was transduced into these cells at least 48 h prior to imaging. mCa^{2+} and $\Delta\Psi_m$ were monitored during 1 h of Ischemia (induced by placing a coverslip) followed by 1 h of reperfusion (removing the coverslip). We analyzed mCa^{2+} levels during I/R by determining the YFP (FRET acceptor emission)/CFP (donor emission) ratio for each cell in the microscopic field (∼100) and repeating the experiment on a minimum of 5 different

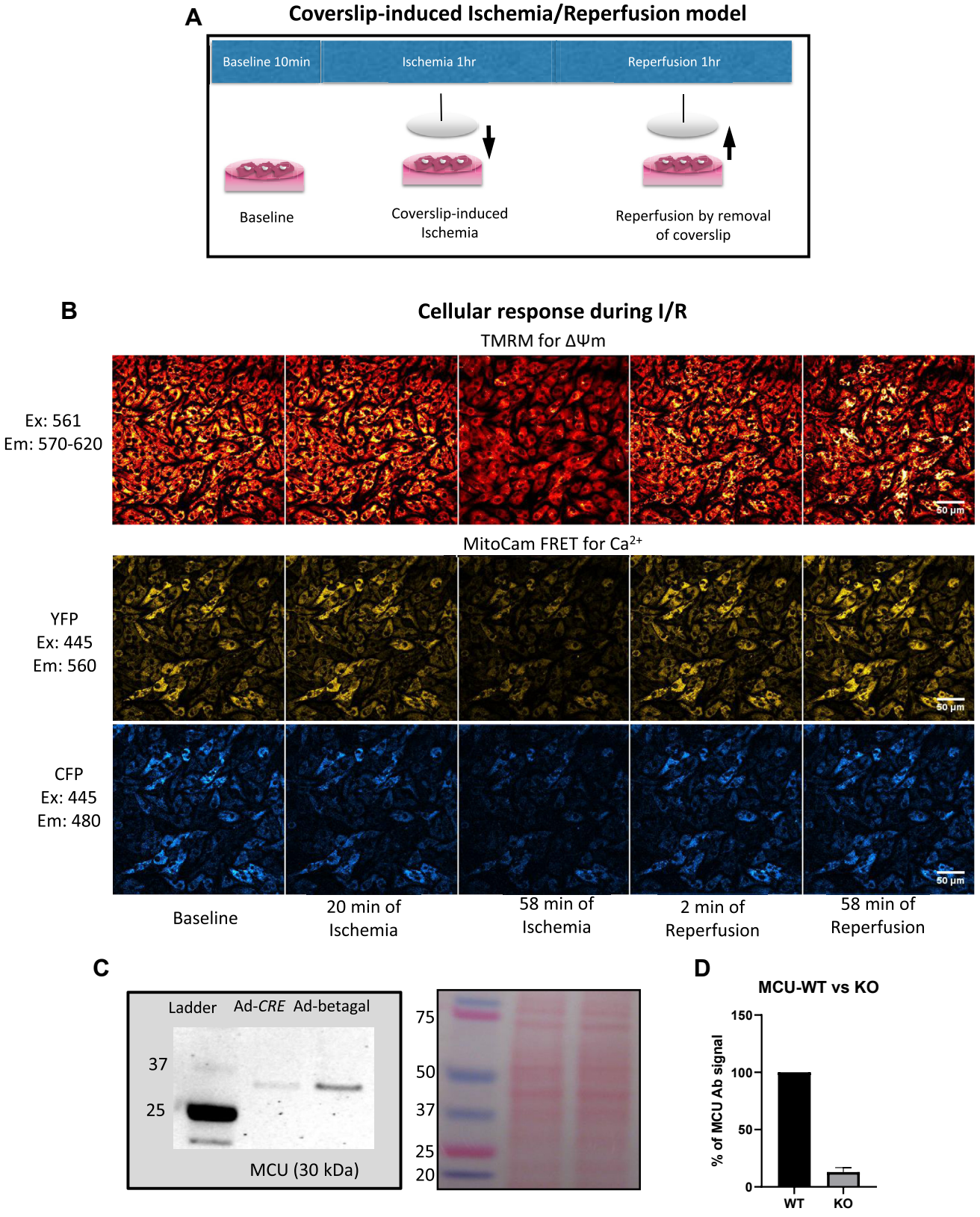

Figure 1. Methods and Protocol. *A*, *In vitro* ischemia and reperfusion protocol on monolayers of neonatal mouse ventricular myocytes (NMVMs). *B*, Representative cellular response during baseline, ischemia, and reperfusion. mitochondrial membrane potential ($\Delta\Psi_m$) and mitochondrial Ca^{2+} were monitored with TMRM and the genetically encoded MitoCam (4mtd3cpv) FRET probe, respectively. TMRM fluorescence was excited at 561 nm and emission was collected from 570 to 620 nm. For MitoCam, CFP was excited at 445 nm and emission was collected at 480 nm. The FRET signal (YFP) was collected at 560 nm. The ratio of the FRET signal to CFP after background subtraction indicated mCa^{2+} levels. *C*, NMVMs from $MCU^{fl/fl}$ mice were transduced with adenovirus expressing *Cre*-recombinase (Ad-Cre) or βgal (Ad-βgal) control virus. *Left panel*: 80% reduction in MCU protein (expected molecular weight of 30 kDa) observed on the fifth day after viral transduction in Ad-Cre treated cells. *Right Panel*: Ponceau stained loading control. *D*, Quantification of MCU protein from western blots (n = 6). MCU, mitochondrial calcium uniporter.

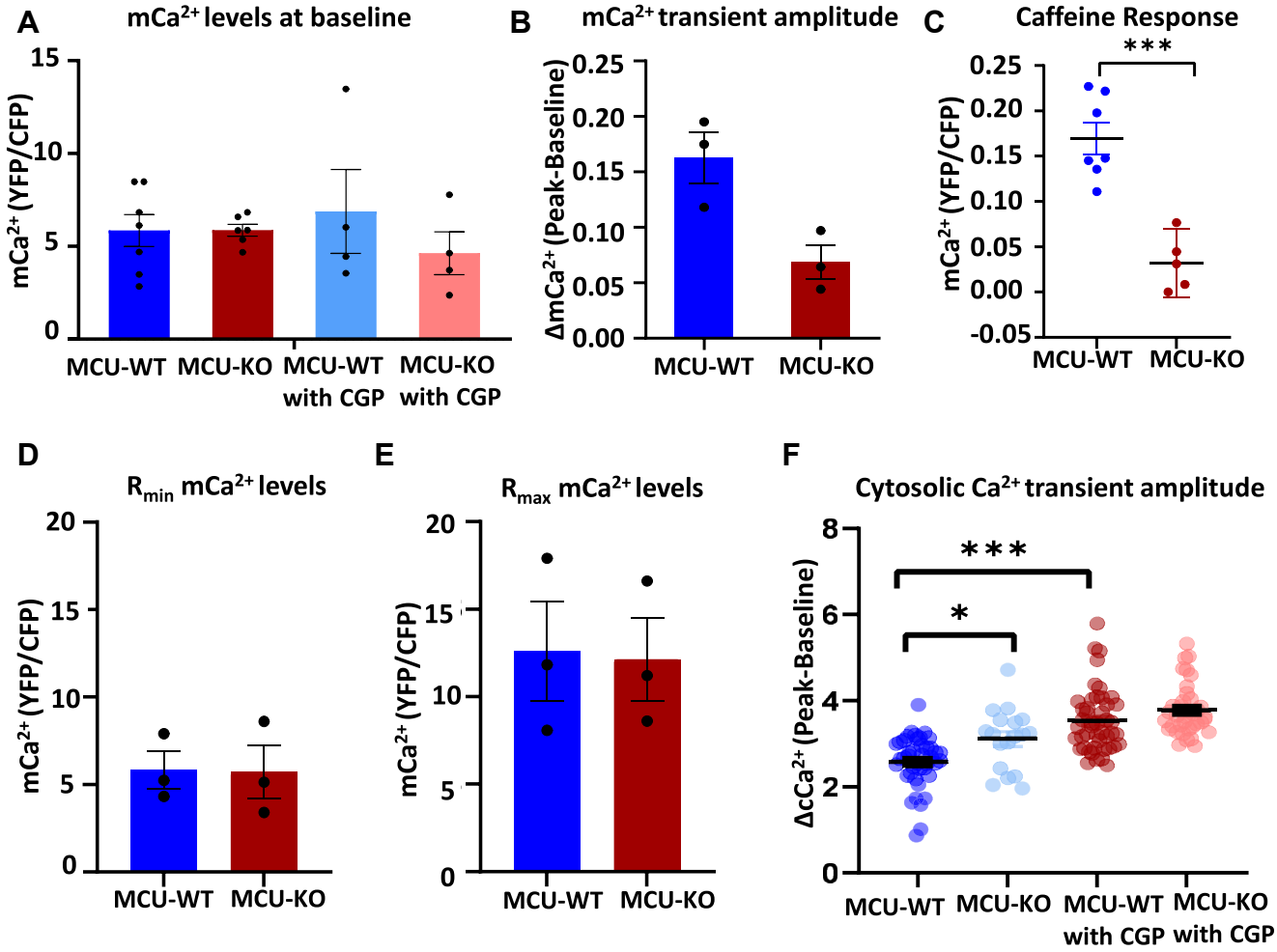

Figure 2. MCU is required for rapid Ca^{2+} uptake into mitochondria. *A*, mCa^{2+} levels at baseline in Neonatal Mouse Ventricular Myocytes using the MitoCam probe. mCa^{2+} levels are represented as a ratio of the FRET signal (YFP) to CFP. Baseline mCa^{2+} for MCU-WT, MCU-KO, as well as MCU-WT or MCU-KO in the presence of CGP-37157 (CGP; 10 μM). *B*, mCa^{2+} transient amplitude in unstimulated cells in MCU-WT and KO. *C*, mCa^{2+} uptake measured when SR-Ca^{2+} is released by caffeine in the presence of 0 mM Na^{+} (Welch's *t* test, WT= 7, KO= 5 cells). *D* and *E*, Rmin and Rmax levels for MitoCam signal in both groups. *F*, Cytosolic Ca^{2+} transients measured using Fura-2, with and without CGP. N > 18 cells (Kruskal Wallis non-parametric test, with Dunn's Multiple comparison). Experiments (and calibrations) were repeated at least 3 times. Mean ± SEM is shown. KO, knockout; MCU, mitochondrial calcium uniporter; WT, wild type.

preparations. We observed that there was no correlation between MitoCam expression and the characteristics of the mCa^{2+} response, ruling out possible differences due to direct buffering by MitoCam. Example traces of mCa^{2+} during I/R (included in Fig. S3) show the consistent behavior of all cardiomyocytes in the NMVM monolayer. We observed a rise in Ca^{2+} levels during early ischemia up to ~25 min, after which mCa^{2+} levels declined in both MCU-WT and MCU-KO cells (Fig. 3, *A* and *C*), in parallel with loss of $\Delta\Psi_m$ (Fig. 3*E*). At the end of ischemia, mCa^{2+} levels were lower than at baseline. No significant differences were observed in mCa^{2+} levels between MCU-WT and MCU-KO during the early (2–3 min), maximum, and end (last minute) of the ischemic phase (Fig. 3*C*).

Immediately upon reperfusion, mCa^{2+} influx was observed in both MCU-WT and MCU-KO cardiomyocytes. No significant differences were found in mCa^{2+} levels between MCU-WT and MCU-KO cells at early (first minute), mid (29–31 min), or end (last minute) of the reperfusion phase (Fig. 3*D*). We then tested whether inhibition of mNCE had effects on mCa^{2+} and $\Delta\Psi_m$ during I/R. We found that CGP significantly abolished the rise of mCa^{2+} in early ischemia and greatly suppressed mCa^{2+} influx during reperfusion (although this suppression was not significantly different between CGP-treated and untreated cells) (Fig. 3, *B* and *C*). Although the ischemia-induced early rise in mCa^{2+} levels was suppressed, mCa^{2+} at the end of Ischemia was not significantly different in CGP-treated *versus* untreated cells. We also measured cytosolic Ca^{2+} with a genetically encoded cytoplasmic Ca^{2+} probe (d3cpv), with or without CGP, and confirmed that the CGP effect was not attributable to inhibition of cytoplasmic Ca^{2+} levels during I/R (Fig. S4). To determine if CGP was indirectly suppressing mCa^{2+} uptake by disrupting $\Delta\Psi_m$, we also monitored $\Delta\Psi_m$ changes simultaneously with mCa^{2+} during the I/R period. The observed changes in mCa^{2+} uptake in CGP-treated cells were not due to altered $\Delta\Psi_m$ responses. These results indicate that the mNCE mediates mitochondrial Ca^{2+} uptake during Ischemia.

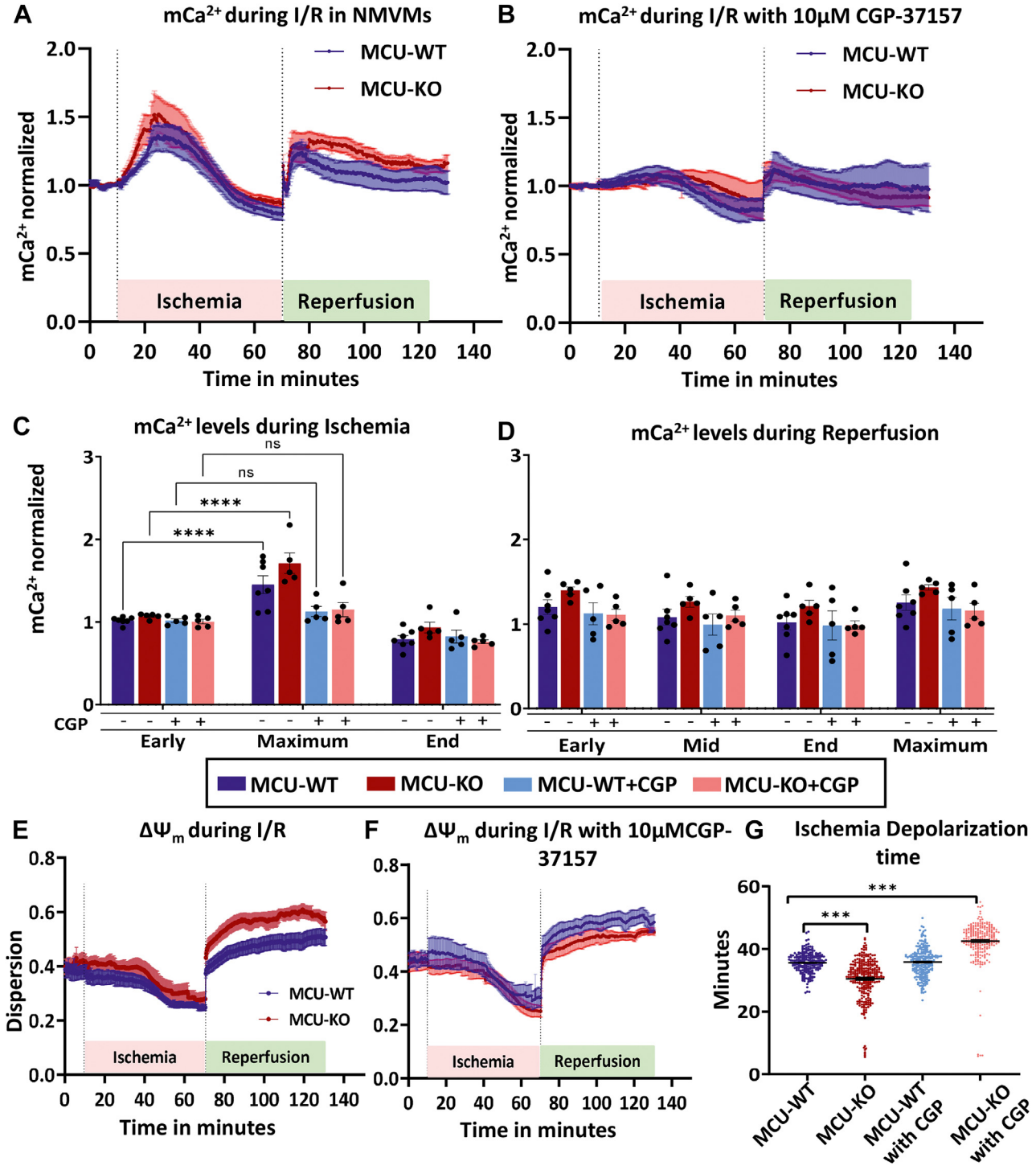

Figure 3. MCU knockout does not affect mitochondrial Ca^{2+} import during Ischemia and Reperfusion but blocking mNCE prevents the rise in mCa^{2+} during Ischemia. *A*, Mitochondrial Calcium monitored in Neonatal Mouse Ventricular Myocytes in control (MCU-WT) or knockout myocytes (MCU-KO) during 1 h of ischemia and 1 h of reperfusion. mCa^{2+} for each cell was quantified by obtaining the YFP/CFP ratio and normalizing to pre-ischemia baseline. *B*, mCa^{2+} in MCU-WT and MCU-KO cells in the presence of CGP-37157 (10 µM). *C* and *D*, Quantification of mCa^{2+} levels at different stages during Ischemia and Reperfusion. Number of experiments, WT(7), KO(6), WT+CGP(5), KO+CGP(5). Mean ± SEM are plotted. 2-way ANOVA was performed between treatments (***$p < 0.05$). *E*, $\Delta\Psi_m$ changes during I/R were assessed by measuring spatial TMRM signal Dispersion in each individual cell and then averaging the response for each experiment. $\Delta\Psi_m$ in control MCU-WT (*blue*) and MCU-KO myocytes (*red*) throughout Ischemia/Reperfusion. *F*, $\Delta\Psi_m$ response in MCU-WT and MCU-KO myocytes in the presence of CGP-37157 (10 µM) throughout Ischemia/Reperfusion. *G*,Time to $\Delta\Psi_m$ depolarization during Ischemia in WT, KO and CGP-treated cells. SEM is indicated in *F* and *G*. KO, knockout; MCU, mitochondrial calcium uniporter; WT, wild type.

Mitochondrial Oscillations on Reperfusion

MCU-KO does not protect against $\Delta\Psi_m$ loss during I/R nor does inhibition of mNCE

$\Delta\Psi_m$ changes were assessed by plotting the TMRM dispersion for each individual cell during 1 h of ischemia and 1 h of reperfusion. This measure minimizes potential artifacts due to dye loading variability and fluorescence decay over the experimental time course. $\Delta\Psi_m$ decreased biphasically during ischemia, consistent with visual observations of TMRM redistribution within the cells. Upon reperfusion, $\Delta\Psi_m$ repolarized within the first minute of coverslip removal, followed by heterogeneous $\Delta\Psi_m$ oscillation across the microscopic field (Video S1). When we compared the $\Delta\Psi_m$ response in MCU-WT to MCU-KO NMVMs, or to CGP-treated monolayers, we observed no significant difference in the pattern of behavior between the different groups (Fig. 3, *E* and *F*). Although MCU-KO myocytes showed somewhat higher average dispersion values on reperfusion, closer examination of the images indicated that this was due to an increase in the spatial heterogeneity of the mitochondrial network within cells, rather than an actual increase in $\Delta\Psi_m$ of polarized mitochondria in the MCU-KO group, that is, there was a slight increase in variation in signal across the cell as a consequence of abundant mitochondrial $\Delta\Psi_m$ oscillations (Video S2).

It is important to note that the dispersion measurement gives us a broad representation of $\Delta\Psi_m$ across the coverslip but does not facilitate the identification of the transition states of $\Delta\Psi_m$ polarization and depolarization in individual cells. Hence, we tracked each cell's TMRM fluorescence and assessed $\Delta\Psi_m$ changes at the single-cell level during ischemia and reperfusion, applying MitoWave, a wavelet transform signal processing method we recently developed (35), to automatically detect transition points during ischemia and frequency components of $\Delta\Psi_m$ instability on reperfusion. Interestingly, MCU knockout was found to accelerate the time to $\Delta\Psi_m$ loss during ischemia indicating greater susceptibility, while CGP delayed the time to Ischemic $\Delta\Psi_m$ loss in MCU-KO cells. This ischemic prolongation effect by CGP was not observed in MCU-WT cells (Fig. 3*G*). This increased susceptibility to CGP in MCU-KO monolayers could suggest an increase in the expression of NCLX, the protein underlying mNCE; however, NCLX expression levels did not differ between MCU-KO and WT cells (Fig. S10).

Next, we determined if modulating mCa^{2+} influx affects $\Delta\Psi_m$ instability during reperfusion. $\Delta\Psi_m$ instability during reperfusion is a hallmark of mitochondrial damage that could translate to higher organ-level arrhythmias (23). Since $\Delta\Psi_m$ oscillations during reperfusion are non-stationary, we also used the MitoWave method (35) for an unbiased approach to quantitatively analyze and categorize $\Delta\Psi_m$ oscillatory behavior during reperfusion. Continuous wavelet transform enabled the determination of the dominant frequencies displayed by individual mitochondrial clusters over the duration of reperfusion (Fig. 4). We further classified $\Delta\Psi_m$ oscillatory behaviors by separating them into frequency bands. High-frequency oscillators fell into the top two bands of 45 to 8.6 and 8.6 to 4.3 mHz (oscillations periods of 22–116 s and 116–230 s, respectively), moderately fast frequencies ranging from 4.3 to 2.2 mHz (230–450 s), and low-frequency oscillators of less than 2.2 mHz (>450 s), largely representing stable polarized mitochondria. The time at which a mitochondrion underwent irreversible $\Delta\Psi_m$ collapse during reperfusion was also included in this analysis. Figure 4, *A–D* shows scalograms of representative individual mitochondria from WT, KO, WT+CGP, or KO+CGP NMVMs during reperfusion. High coefficient peaks are present in the low scale range of 1 to 10 with all the interventions. We next plotted the frequency components of all the mitochondrial clusters as violin plots. Each dot on the violin plot represents the behavior of a mitochondrial cluster in a given time window during reperfusion, and any individual mitochondrial oscillator can appear in different frequency bands if its behavior shifts over time (*e.g.*, the mitochondrial cluster might transition from the high-frequency band to the lowest band if it stops oscillating). Importantly, knocking out MCU did not prevent high-frequency $\Delta\Psi_m$ oscillations during reperfusion (Fig. 4, *A*, *B*, *E*, and *F* and Videos S1 and S2), that is, high-frequency oscillators were present in the top two bands throughout the reperfusion period (Fig. 4, *E* and *F*). Treatment with CGP suppressed mCa^{2+} uptake during IR; however, it did not prevent $\Delta\Psi_m$ oscillations on reperfusion, and there were no significant differences in the patterns of $\Delta\Psi_m$ oscillatory behavior with CGP treatment (Fig. 4, *C*, *D*, *G* and *H* and Videos S3 and S4).

Taken together, these results suggest that: (1) knocking out MCU does not affect mitochondrial membrane potential instability during I/R injury; (2) MCU is not the primary mode of mCa^{2+} influx into mitochondria during ischemia; instead, it is mediated by reverse-mode mitochondrial Na^+/Ca^{2+} exchange; and (3) $\Delta\Psi_m$ instability upon reperfusion is independent of mCa^{2+} influx.

Blocking mitochondrial electron transport chain component complex I stabilizes early $\Delta\Psi_m$ oscillations during reperfusion in WT cells

Complex I is the first electron acceptor in the mitochondrial respiratory chain and can control the rate of electron redirection to superoxide. During reperfusion after ischemic injury, ROS production from the mitochondrial respiratory chain is a major source of oxidative damage. Previously, we showed that rotenone treatment, as well as other electron transport chain inhibitors (except the complex III inhibitor antimycin A), stabilized laser-induced ΔΨm oscillations in adult guinea pig cardiac myocytes while decreasing ROS(17). Knocking out Ndufs4h of complex-1 also reduced the number of mitochondrial "flashes" in Langendorff-perfused hearts (36). Therefore, we tested whether inhibition of complex I, with 1 μM rotenone applied at the moment of reperfusion, had any effects on mitochondrial oscillations. We found that rotenone treatment during reperfusion resulted in mitochondrial $\Delta\Psi_m$ oscillations transitioning to a stable polarized state within the first 5 to 10 min, (Figs. 5*C* and S5*A* and Video S5). However, after 20 min of reperfusion, mitochondria started to permanently depolarize in the presence of rotenone, presumably as a consequence of the loss of proton pumping capability by

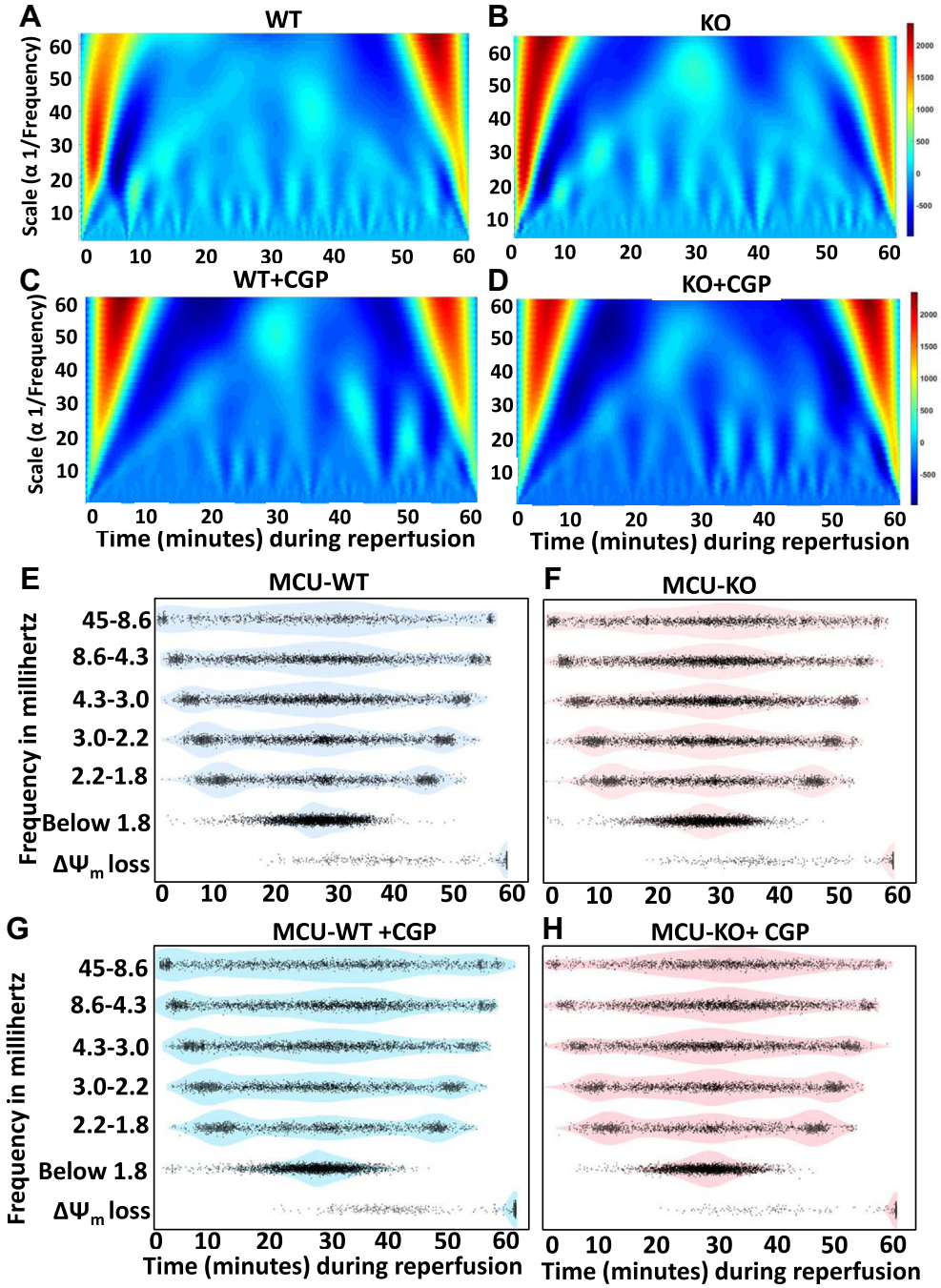

Figure 4. Mitochondrial oscillations persist when MCU is knocked out or with addition of CGP-37157. *A–D*, Representative scalograms of oscillating mitochondrial clusters in the 60-min reperfusion phase showing the presence of peak coefficients in the low scale range of 1–10 or high-frequency range corresponding to 45–8.6 and 8.6–4.3 mHz bands. Scalograms from mitochondrial clusters from WT, KO, WT+ CGP, and KO+ CGP treated cells are shown. They all show persistent oscillations in the 45–8.6 and 8.6–4.3 mHz bands. *E–H*, Violin dot plots showing the frequency distribution of oscillating clusters throughout the reperfusion phase determined by wavelet analysis for each experimental condition. Six frequency bands ranging from the fastest (45–8.6 mHz) to the slowest (Below 1.8 mHz) are shown. The time to irreversible $\Delta\Psi_m$ depolarization is indicated as the lowest band. *A*, frequency distribution during reperfusion of oscillating mitochondrial clusters from WT cells (4093 mitochondrial clusters were analyzed from 7 different I/R of monolayers). *B*, frequency distribution from oscillating mitochondrial clusters from MCU-KO cells (3643 clusters from 6 different I/R of monolayers); *C*, from MCU-WT cells treated with CGP (3208 clusters from 5 different I/R of monolayers); *D*, MCU-KO cells treated with CGP (2977 clusters from 5 different I/R of monolayers were analyzed). KO, knockout; MCU, mitochondrial calcium uniporter; WT, wild type.

complex I and depletion of alternative electron donors to the respiratory chain that may have supported $\Delta\Psi_m$ (Figs. 5A and S5A and Video S5). Fig. S5*A* is a scalogram of a representative mitochondrion during reperfusion. A large spike of scalogram coefficients occurs around ∼25 min of reperfusion when the mitochondrion has undergone complete $\Delta\Psi_m$ depolarization. Ischemic mCa^{2+} uptake during ischemia was not different from controls in this experiment because rotenone was added only at reperfusion. During reperfusion, there was a decrease in mCa^{2+} uptake, presumably because of the loss of $\Delta\Psi_m$

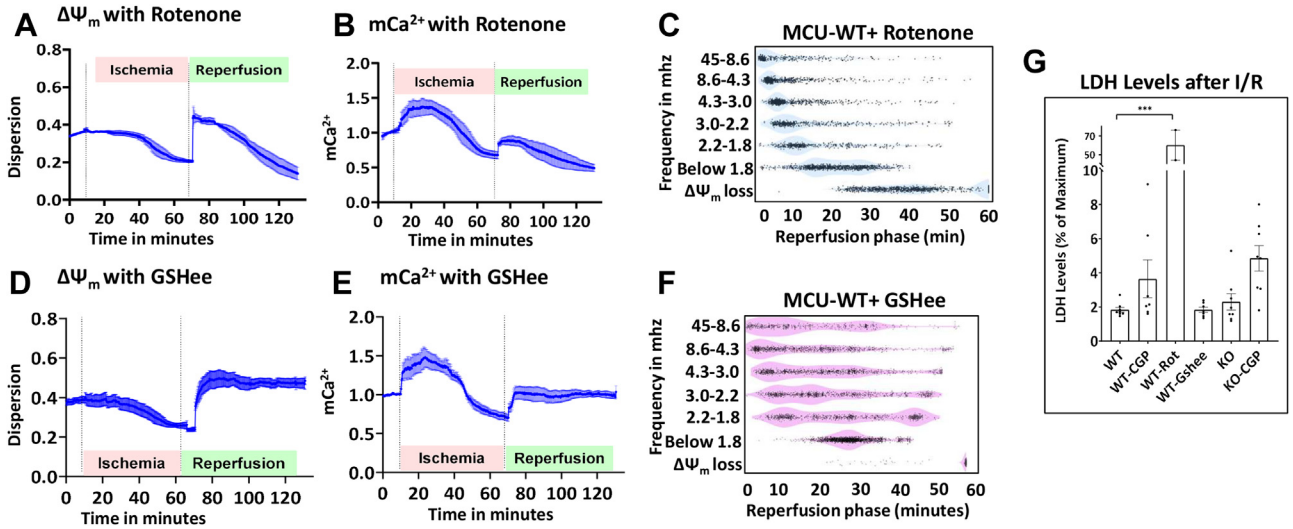

Figure 5. Inhibiting mitochondrial oxidative phosphorylation at complex I or increasing reduced glutathione stabilizes ΔΨm oscillations during reperfusion in MCU-WT cells. *A*, ΔΨm response with Rotenone (1 mM) added upon reperfusion. Inhibition of complex I facilitated ΔΨm stabilization during the first 20 min of reperfusion but increased sustained ΔΨm loss thereafter. *B*, mCa^{2+} recovery was blunted when Rotenone was added upon reperfusion. *C*, Violin dot plots representing frequency distribution oscillating mitochondrial clusters during reperfusion. The number of high-frequency oscillators (in the 45–8.6 and 8.6–4.3 mHz bands) was decreased by Rotenone over the first 20 min of reperfusion. Sustained ΔΨm loss began after 20 min of reperfusion as indicated by the increased density of points in the lowest band. Mean ± SEM are shown in the time course plots. Three different coverslips and 1685 clusters were analyzed for their oscillation patterns. *D–F*, Pre-treatment with the cell-permeable glutathione ethyl ester (GSHee; 4 mM) for 3 h did not affect the mean ΔΨm (*D*) or mCa^{2+} (*E*) responses during I/R, but GSHee mediated stabilization of high frequency oscillators (evident as a decreased density of points in the 4.3–45 mHz band and an increase in the Below 1.8 mHz band) by 20 to 40 min of reperfusion and prevented sustained ΔΨm loss (*F*). Four coverslip experiments with 2020 mitochondrial clusters analyzed for oscillatory patterns. *G*, LDH Assay as a measure of cytotoxicity at the end of Reperfusion after Ischemia. Supernatants were collected after reperfusion to measure Lactate Dehydrogenase levels. Positive control was supernatant from lysed NMVMs and was considered as 100% of LDH levels released (maximum). One-way ANOVA comparing WT with rotenone treatment showed significantly elevated levels of LDH at the end of I/R. WT comparisons with other samples were not significantly different. GSHee, reduced Glutathione; LDH, Lactate Dehydrogenase; MCU, mitochondrial calcium uniporter; NMVMs, neonatal mouse ventricular myocytes.

(Fig. 5*B*). We further tested the effects of pre-I/R treatment with a cell-permeable form of the complex II substrate dimethyl succinate (5 mM, added 10 min before I/R) to bypass complex I inhibition in the presence of rotenone (Fig. S6). $\Delta\Psi_m$ oscillations still occurred in some mitochondria under these conditions (Figs. S6*C* and S5*C* and Video S8). We observed a few low coefficient peaks in the scalogram before the mitochondria underwent complete $\Delta\Psi_m$ depolarization at 20 to 30 min. This suggests that bypassing complex I and supplying electrons *via* complex II can partially reactivate the oscillatory mechanism, perhaps by restoring ROS emission from complexes of the Electron Transport Chain (ETC) downstream of complex I, namely, complexes II, III or IV.

Supplementing NMVMs with cell-permeable glutathione stabilizes $\Delta\Psi_m$ oscillations during reperfusion

Given the lack of effect of interventions affecting mCa^{2+}, we next tested the hypothesis that ROS was the primary trigger for $\Delta\Psi_m$ oscillations on reperfusion. A cell-permeable (ethyl ester) form of reduced Glutathione (GSHee) was used to increase intracellular glutathione reserves. NMVMs were preincubated with 4 mM GSHee for 3 h before replacing the media with normal Tyrode's to perform the I/R protocol while monitoring mCa^{2+} and $\Delta\Psi_m$. We observed the initial rise of mCa^{2+} during ischemia as expected, and the increase in mCa^{2+} upon reperfusion as well (Fig. 5*E*). The global average $\Delta\Psi_m$ response throughout the I/R period was not substantially different (Fig. 5*D*); however, $\Delta\Psi_m$ oscillations stabilized after 20 min of reperfusion (Figs. 5*F* and S5*B* and Video S6) and $\Delta\Psi_m$ was well maintained for the majority of mitochondria over the 1-h reperfusion period.

Inhibition or knockout of cyclophilin D does not prevent $\Delta\Psi_m$ oscillations

Mitochondrial permeability transition pore opening has been implicated in mitochondrial dysfunction to precipitate cell death during reperfusion. Cyclophilin D (encoded by the *ppif* gene) is a mitochondrial matrix peptidylprolyl isomerase that participates in gating the mPTP pore (37). Cyclosporine A inhibits cyclophilin D interaction with mPTP and desensitizes its Ca^{2+}-dependent activation (38, 39). We tested whether Cyclosporine A (CsA) improved $\Delta\Psi_m$ recovery and mCa^{2+} changes during I/R and found no salutary effect (Fig. S7, *A* and *C*). CsA also did not prevent $\Delta\Psi_m$ oscillations (Figs. S7 and S5*D* and Video S7). To further confirm the mPTP independence of reperfusion-induced $\Delta\Psi_m$ oscillations, we also performed *in vitro* I/R experiments in NMVMs isolated from *ppif* gene-null neonatal mice and found no protective effect of *ppif* gene knockout (Fig. S8*A* and *C*.). On the contrary, during reperfusion, *ppif* knockout NMVMs fared worse than WT controls—we observed irreversible $\Delta\Psi_m$ collapse peaking at 30 to 40 min of reperfusion and complete loss of $\Delta\Psi_m$ by 1 h (Fig. S8 and Video S9). In *ppif* knockout NMVMs, mCa^{2+} levels increased during ischemia with similar kinetics but did

not return to baseline at the beginning of reperfusion (Fig. S8*B*), although $\Delta\Psi_m$ recovered during early reperfusion. Knocking out the *ppif* gene also did not prevent $\Delta\Psi_m$ oscillations (Figs. S8*C* and S5*E* and Video S9).

The behavior of high-frequency oscillators under different conditions

The overall behavior of $\Delta\Psi_m$ oscillations during reperfusion is shown in Figures 4, *E–H* and 5, *C* and *F*. Mitochondrial oscillators were separated into three main frequency bands and observed that a mitochondrion can switch its frequency during reperfusion. Further, we examined the number of mitochondrial clusters that changed from fast frequency to slower frequency with different treatments as well as the number of mitochondrial clusters that irreversibly lost $\Delta\Psi_m$ during reperfusion (Fig. 6, *A–F*). Further, we statistically analyzed the effect of different conditions on high-frequency oscillators (in the 8.6–45 mHz frequency band) to see how they vary throughout reperfusion time. Empirical Cumulative Distribution (ECDF) functions of the high-frequency oscillators, reflecting the cumulative probability of mitochondria leaving the high-frequency state (either to a stable $\Delta\Psi_m$ polarized state or completely depolarized state) during reperfusion, were plotted against the reperfusion time (Fig. S9*C*) for statistical comparison by non-parametric Kolmogorov–Smirnov test, where the null hypothesis is that the distribution of mitochondrial oscillators under different treatments does not change over the course of reperfusion (Fig. 6*G*). While knocking out MCU or addition of CGP (effectively suppressing mCa^{2+} influx) did not affect the high-frequency oscillations (p = not significant, with alpha = 0.001), modulating ROS production (*via* inhibition of electron transport) or increasing the antioxidant capacity of the cells, suppressed the high-frequency oscillators ($p < 0.000001$). Over the course of reperfusion, $\Delta\Psi_m$ was optimally stabilized and maintained when the antioxidant pool was supplemented by GSHee treatment. Ppif knockout also shifted the ECDF curve to the left; however, as described earlier, this was reflective of the earlier complete collapse of $\Delta\Psi_m$ rather than the stabilization of the oscillators in the polarized state. Thus, we observed that the high-frequency oscillators are strongly influenced by either blocking the electron transport chain with rotenone or by replenishing the glutathione pool with a cell-permeable glutathione ethyl ester.

We further analyzed lactate dehydrogenase (LDH) levels in supernatants as a marker for cytotoxicity after reperfusion injury (Fig. 5*H*). LDH levels were not significantly different between MCU WT and KO cells. CGP or GSHee addition did not affect cytotoxicity levels. Although the addition of rotenone stabilized early $\Delta\Psi_m$ oscillations, it significantly increased LDH levels, as expected, since inhibition of the ETC inhibits oxidative phosphorylation and ATP production and exacerbated irreversible $\Delta\Psi_m$ loss on reperfusion.

Taken together, these results show that $\Delta\Psi_m$ oscillations that occur during reperfusion after ischemia are triggered by ROS and not by mCa^{2+}.

Discussion

It is commonly held that excess mitochondrial Ca^{2+} loading during or after ischemia is the major contributor to mitochondrial loss of function, and subsequent tissue damage on reperfusion. Nevertheless, the difficulty of accurately measuring mitochondrial Ca^{2+} in models of cardiac IR have prevented a definitive exploration of the modes of mCa^{2+} uptake and release and the mechanisms triggering mitochondrial $\Delta\Psi_m$ instability on reperfusion. Here, we leveraged the rapid MCU knockout model in a cardiomyocyte monolayer and the ability to easily monitor $\Delta\Psi_m$ and mCa^{2+} simultaneously during I/R to directly address the relationship between mCa^{2+} and $\Delta\Psi_m$ behavior under stress. The major conclusions of the study were that: (1) the primary trigger for $\Delta\Psi_m$ instability during reperfusion is reactive oxygen species rather than mCa^{2+}, and (2) under ischemic conditions, mNCE, not MCU, is the primary mode of Ca^{2+} import into mitochondria. The findings challenge current paradigms of I/R injury, which may lead to new therapeutic approaches in the future.

Role of MCU and mNCE during ischemia/reperfusion

Excess accumulation of Ca^{2+} is thought to trigger mitochondrial permeability transition pore opening leading to cell death (40–42). Several studies have shown that during ischemia, Ca^{2+} in mitochondria increases (9). It has been generally assumed that Ca^{2+} overload of mitochondria, in this case, occurs through the mitochondrial calcium uniporter (5–7). In line with this thinking, it was shown that inhibiting the MCU either chemically, with Ru360, or genetically knocking out the cardiac-specific MCU had protective effects on IR injury (12, 13, 43). However global MCU-KO, or even cardiac-specific expression of a dominant negative MCU, did not show any protection in myocardial injury compared to WT mice (10, 11). Our approach was to acutely knockout (in ~5 days of cell culture) MCU to prevent any long-term adaptations in the hope of explaining this inconsistency. We found reduced mCa^{2+} transients in beating cells, consistent with findings from other laboratories showing suppression of mCa^{2+} transients in neonatal rat cardiomyocytes with MCU knocked down (33).

We found no differences in basal mCa^{2+} levels in our acute MCU-KO model. Similarly, Kwong *et. al.* also found no differences in the matrix [Ca^{2+}] in isolated cardiac mitochondria as well as in permeabilized cardiomyocytes (13) in an adult cardiac-specific MCU-KO model. In contrast, Holmström *et. al.* (44) found a 75% decrease in matrix Ca^{2+} levels in isolated mitochondria from global MCU KO cardiomyocytes. These data demonstrate that knocking out MCU does not necessarily eliminate Ca^{2+} influx into the mitochondria, indicating that other pathways might contribute to mCa^{2+} influx.

Indeed, Fieni *et al.* (30) showed that the amount of Ca^{2+} uptake mediated by the MCU varies between tissues, and MCU current density was the smallest in the heart mitochondria (30). The ratio of MCU to its dominant negative form, MCUb, varies among different tissues. For example, in the heart it is 3:1 (MCU:MCUb), and in skeletal muscle it is

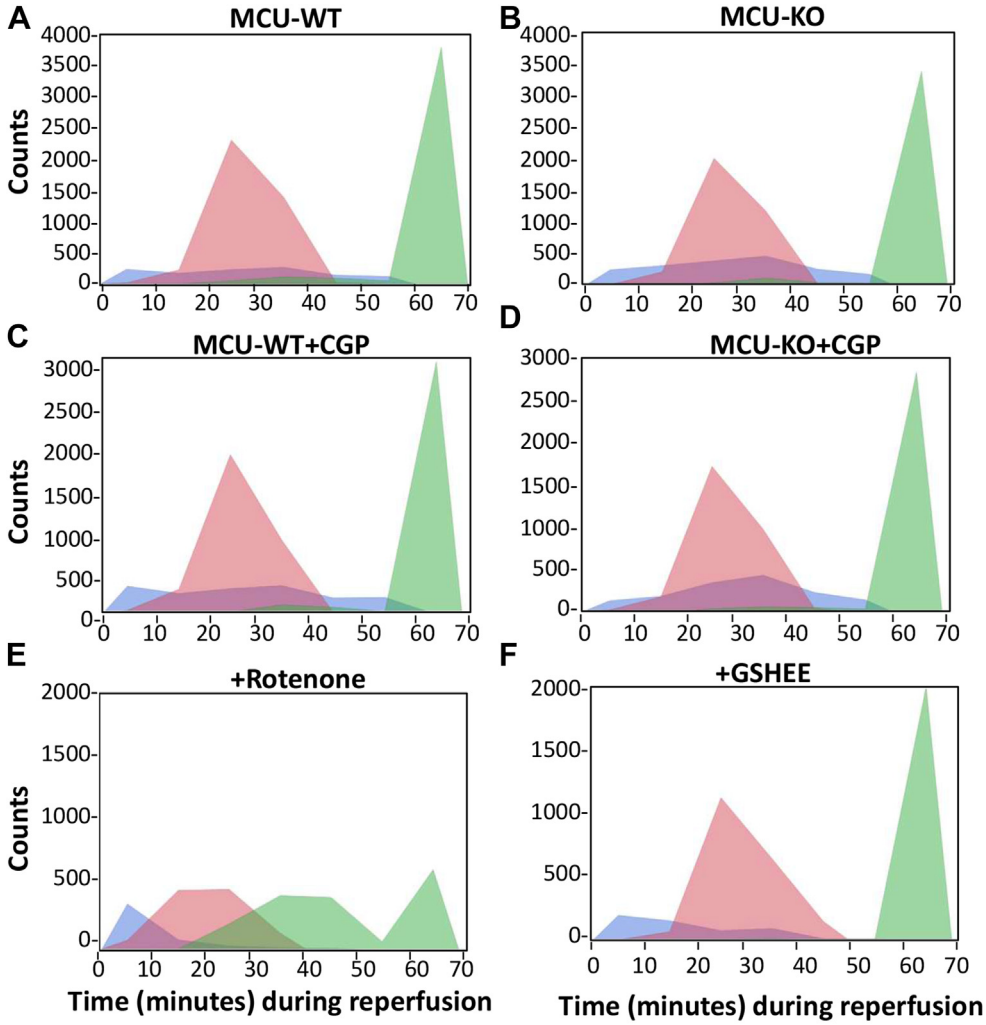

G

Non-parametric Kolmogorov-Smirnov test (Alpha = 0.001)		No. of clusters	No. of I/R experiments
MCU-WT vs MCU-KO	0.0019	4093(WT) 3643(KO)	7(WT), 6(KO)
MCU-WT vs WT with CGP	0.1269	3208 (WT+CGP)	5
MCU-WT vs WT with GSHee	9.4218e-33	2020 (WT+GSHee)	4
MCU-WT vs WT with Rotenone	4.8009e-104	1685 (WT+Rotenone)	3

Figure 6. Redistribution of $\Delta\Psi_m$ oscillation frequency during Reperfusion. *A–D*, Counts of mitochondrial clusters changing between fast (45–8.6 mHz; *blue* polygonal histogram) and slow frequencies (below 1.8 mHz; *pink* polygonal histogram) over the reperfusion time period with different treatments. Counts of mitochondrial clusters undergoing $\Delta\Psi_m$ loss are also shown (*green* polygonal histogram). No significant differences were observed between MCU-WT, MCU-KO, and CGP treatment groups (*G*). *E–F*, with Rotenone treatment (*E*), the counts of fast oscillators decreased at 10 to 15-min time point while the count of slow oscillators increase. However, these mitochondria did not sustain $\Delta\Psi_m$, with irreversible depolarization starting at 15 min of reperfusion. With anti-oxidant glutathione ethyl ester (GSHEE) treatment (*F*), the number of fast oscillators decreased, starting around 15 min of reperfusion while the number of slow oscillators increased. $\Delta\Psi_m$ loss occurred (if at all) only after 55 min of reperfusion. *G*, significant differences were observed between MCU-WT and GSHEE treatment and MCU-WT and Rotenone treatment. A non-parametric Kolmogorov–Smirnov test with alpha =0.001 was performed to test for significance. KO, knockout; MCU, mitochondrial calcium uniporter; WT, wild type.

40:1 (45), thus resulting in differential regulation of Ca^{2+} into mitochondria. In addition, other modes of Ca^{2+} entry into the mitochondria have been proposed, such as through the mitochondrial ryanodine receptor (46, 47) and the LETM1-Ca^{2+}/H^{+} exchanger (48, 49). Moreover, under ischemic conditions, reversal of the mitochondrial $Na^{+}/Ca^{2+}/Li^{+}$ exchanger

might allow Ca^{2+} entry into the mitochondria, as previously proposed (50). Furthermore, Nicholls *et al* (51) showed that above a load of 10 nmol Ca^{2+}/mg of mitochondrial protein, matrix free Ca^{2+} (which the MitoCam probe detects) is buffered to a limiting concentration of 1 to 5 μM despite additional uptake. Therefore, several factors could take precedence in influencing measured mCa^{2+} levels, especially when MCU is impaired.

Surprisingly, our *in vitro* I/R myocyte monolayers showed no difference in Ca^{2+} uptake between MCU-KO and WT during ischemia as well as during reperfusion. Ca^{2+} influx *via* MCU requires maintenance of $\Delta\Psi_m$ (5, 52), which, in our experiments, was lost after 30 min of ischemia; however, the maximum Ca^{2+} increase during ischemia occurred before the loss of $\Delta\Psi_m$, and this peak was also unaffected by MCU knockout. This suggests that other factors may be restricting MCU-mediated Ca^{2+} uptake during ischemia. For example, Moreau and Parekh (53) showed that acidification of the mitochondrial matrix inhibits the MCU. In addition, our group previously showed that under conditions of elevated cytosolic Na^+, Ca^{2+} influx into mitochondria is reduced (54). Under Ischemic conditions, there is (*i*) a decrease in pH because of ATP breakdown during increased metabolic demand, (*ii*) $\Delta\Psi_m$ reduction, and (*iii*) elevated cytosolic Na^+ (4). Therefore, ischemic conditions could favor suppression of MCU-mediated mitochondrial Ca^{2+} uptake.

The rise of mCa^{2+} during ischemia was almost completely eliminated by CGP-37157, an inhibitor of the mitochondrial $Na^+/Li^+/Ca^{2+}$ exchanger (55); similarly, mCa^{2+} was also lower upon reperfusion. CGP-37157 is a benzothiazepine with a structure somewhat similar to Ca^{2+} channel blockers, and there are some reports in the literature that it might also inhibit SR Ca^{2+} uptake, ryanodine receptors (56), or L-type Ca^{2+} channels (57). None of these potential off-target effects could explain our results, since there was no significant effect of CGP on the cytosolic Ca^{2+} response to I/R. Previously, Griffiths *et al*. (16), showed that the addition of clonazepam, a benzothiazepine congener that also inhibits mNCE, blunted mCa^{2+} influx during hypoxic conditions, suggesting that mNCE could work in reverse during metabolic inhibition (16). They also reported that mitochondria in adult cardiomyocytes treated with Ruthenium Red (RuR) still took up Ca^{2+} under hypoxic conditions. The putative explanation for this behavior was attributed to the loss of $\Delta\Psi_m$ during ischemia, causing the electrochemical driving force to favor mNCE reversal.

Our *in vitro* cellular model of I/R injury afforded us the opportunity to measure mCa^{2+} ratiometrically, and $\Delta\Psi_m$ simultaneously, during I/R, which is not easily accomplished in whole animal or organ-level model systems. We saw that in both MCU-WT and MCU-KO monolayers, the CGP-sensitive rise in mCa^{2+} occurred early during ischemia when $\Delta\Psi_m$ was still maintained. When $\Delta\Psi_m$ was lost, mitochondrial Ca^{2+} levels rapidly decreased to a level below the normoxic baseline. This indicates that a loss of $\Delta\Psi_m$ cannot account for reverse-mode mNCE activity during early ischemia. With CGP treatment, although mCa^{2+} accumulation was largely suppressed, we did not see any remarkable change in the timing of $\Delta\Psi_m$ loss during ischemia in WT or MCU-KO cells; it still occurred at 30 to 40 min of ischemia. Hence, the early increase in mCa^{2+} is not a determinant of $\Delta\Psi_m$ loss during ischemia nor is the CGP effect on mCa^{2+} related to altered timing of the ischemic $\Delta\Psi_m$ loss.

Possible alterative explanations for mNCE reversal could include an early change in the ionic gradient for Na^+ across the mitochondrial inner membrane, or a shift in the stoichiometry of the Na^+/Ca^{2+} exchanger to an electroneutral mode. In this regard, the electrogenic nature and stoichiometry of mNCE are still debated. The earliest studies favored an electrogenic exchanger when it was found that Ca^{2+} efflux from the mitochondria was dependent on $[Na^+]$ and energy produced from respiration (58, 59). However, some studies favored electroneutral exchange, based on the observation that perturbing $\Delta\Psi_m$ with an uncoupler did not change steady state Ca^{2+} efflux from the mitochondria (60) and that the Na^+ mediated Ca^{2+} efflux process did not perturb $\Delta\Psi_m$ (61). Later studies supported the electrogenic nature of mNCE (62–64). Nevertheless, under conditions of ischemia, changes in $\Delta\Psi_m$, $[Na^+]$, and $[Ca^{2+}]$ could all influence mNCE behavior. Lower Na^+ and higher free Ca^{2+} in the mitochondrial matrix *versus* the cytoplasm, together with $\Delta\Psi_m$, provide the electrochemical driving force to drive Ca^{2+} efflux out of the mitochondria under normal conditions, but under ischemic conditions, it is possible that an electroneutral mode of mNCE takes precedence, leaving only the chemical gradients to determine the direction of ion exchange. The K_m for Na^+ of mNCE has been reported to be ~7 to 10 mM (65–67) and changes in cytosolic Na^+ will affect efflux rates of Ca^{2+} *via* mNCE. During ischemia, cytosolic $[Na^+]$ can reach ~ 40 mM within a few minutes (4), but, unfortunately, we currently have no information about matrix $[Na^+]$, which will be affected by factors including the pH gradient, through the inner membrane Na^+/H^+ exchanger, by mNCE activity, and possibly also by Na^+ leak across the membrane. Similarly, we do not precisely know what the concentration gradient of Ca^{2+} is across the inner membrane. It will be important in the future to get more quantitative information on these gradients to determine how the equilibrium potential for mNCE changes during ischemia. Additional studies will also be required to determine if the CGP-sensitive mitochondrial Ca^{2+} uptake pathway during ischemia is solely mediated by NCLX, the only mitochondrial Na^+/Ca^{2+} exchanger thus far identified.

In summary, our findings indicate that reverse mode mNCE, not MCU, is the primary mode of Ca^{2+} entry during ischemia and early reperfusion, while beat-to-beat mitochondrial Ca^{2+} entry requires MCU.

Ca^{2+} vs ROS in triggering $\Delta\Psi_m$ instability during reperfusion

$\Delta\Psi_m$ instability upon reperfusion can translate to higher organ-level fatal arrhythmias (23). The primary trigger for $\Delta\Psi_m$ instability has been debated, with some groups in support of Ca^{2+}-induced mPTP as the primary mediator of $\Delta\Psi_m$ instability or oscillation (21, 42, 68, 69), while others favor a mechanism involving RIRR, independent of Ca^{2+} (18, 70–72).

Our data in NMVMs support ROS-mediated, Ca^{2+}-independent, $\Delta\Psi_m$ instability. $\Delta\Psi_m$ instability/oscillation characteristics, in terms of frequency or the time to $\Delta\Psi_m$ stabilization, did not differ between MCU-KO and WT, ruling out MCU as the key mediator of oscillation. Furthermore, suppressing the influx of mCa^{2+} with CGP-37157 during ischemia and reperfusion did not alter $\Delta\Psi_m$ instability, providing evidence that the process was Ca^{2+} independent. Indeed, the most effective and reproducible stabilizer of $\Delta\Psi_m$ was the inhibition of the electron transport chain at complex I. A similar effect was observed when NDUFS4, a subunit of complex I was knocked out in mice, *i.e.*, the number of "mito-flashes" was reduced (36). This is somewhat paradoxical, since, in highly reduced isolated mitochondria, inhibition of complex I can increase ROS emission from this site. However, this finding is in agreement with our earlier studies of $\Delta\Psi_m$ oscillations in adult cardiomyocytes, where inhibition of complex I, complex IV (with CN-), complex III (at the Qo site with myxothiazol), or ANT (bongkrekic acid) were all capable of inhibiting oxidative stress and stabilizing whole cell $\Delta\Psi_m$ oscillations (18). The exception was the inhibition of complex III with Antimycin A, which inhibits the Qi site and causes a large increase in superoxide production from complex III. Moreover, as we recently reported in neonatal rat ventricular myocytes (73), the high probability of oscillation during early reperfusion is correlated with a burst of cytosolic oxidative stress, as measured with a genetically encoded probe of the glutathione oxidation state (GRX1-roGFP). Our interpretation of these data is that ETC inhibition either upstream or downstream of complex III prevents RIRR by stopping the source of electron flow to superoxide, and, in turn, H_2O_2. The primacy of ROS in the process is also supported by the effects of supplementation of the cardiomyocytes with a cell-permeable version of reduced glutathione (glutathione ethyl ester; GSHEE), which stabilized $\Delta\Psi_m$ within 20 min of reperfusion. Notably, $\Delta\Psi_m$ oscillatory behavior in adult myocytes is also exquisitely sensitive to the cytoplasmic and mitochondrial GSH:GSSG ratio (20).

Although the *in vitro* myocyte monolayer platform offers advantages in tracking multiple parameters disturbed during I/R at the cellular/subcellular level, and the ability to leverage genetic models for acute gene knockout, limitations of the study include: (*i*) the immaturity of the myocytes, since it is known that metabolism of the neonate is distinctly different from the adult, *e.g.*, being more dependent on glucose than fat oxidation, (*ii*) metabolic differences of mice *versus* humans, and *iii*) the reductionist nature of the approach, which excludes vascular, immune and other factors known to be important in the response to I/R *in vivo*.

Conclusion

We report that during IR, reverse-mode mitochondrial Na^+/Ca^{2+} exchange, not the MCU, is the primary mode of Ca^{2+} import into the mitochondria in Mouse Neonatal Cardiac Myocytes. We also report that $\Delta\Psi_m$ oscillations persist despite blocking mCa^{2+} influx with CGP, showing that $\Delta\Psi_m$ oscillations are not triggered by mCa^{2+} influx. We also show that blocking complex I with rotenone suppresses $\Delta\Psi_m$ oscillations, consistent with a RIRR mechanism. Replenishing the glutathione pool with a cell-permeable reduced glutathione ethyl ester to boost the antioxidant capacity of the system also stabilizes $\Delta\Psi_m$ during reperfusion, reinforcing the conclusion that RIRR is the primary trigger for $\Delta\Psi_m$ instability during reperfusion rather than mCa^{2+} influx. This study provides novel mechanistic insight into mCa^{2+} and $\Delta\Psi_m$ changes during I/R. It has broader significance to translational scientists in highlighting alternative mechanisms of Ca^{2+} import into mitochondria and elucidating how ROS impacts mitochondrial $\Delta\Psi_m$ temporal instability upon recovery from ischemic injury.

Experimental procedures

Mouse models

We are grateful for the generous contributions of genetically engineered mice from colonies maintained in the laboratories of Dr John Elrod and Dr Elizabeth Murphy. The MCU Floxed mice (RRID:IMSR_JAX:029,817), obtained from Dr Elrod's laboratory (12, 13), are conditional knockout mice generated by recombinant insertion of a targeting gene containing loxP sites flanking the fifth and sixth exon of the MCU gene in mouse embryonic stem cells. Breeding pairs were obtained from Dr Elrod and neonates were isolated in our lab to prepare neonatal mouse ventricular myocytes. Breeder mice with global *ppif* (encoding Cyclophilin D) knockout, in which the first three coding exons were replaced with a neomycin resistance cassette (RRID:IMSR_JAX:009,071) were obtained from the laboratory of Dr Murphy and NMVMs prepared using the same protocol. Both mouse lines were originally derived in the laboratory of Dr Jeff Molkentin. All animal procedures were approved by IACUC.

Neonatal cardiomyocyte isolation, cell culture, and adenoviral transfection

Neonatal mouse ventricular myocytes (NMVMs) were isolated using MACS Miltenyi Biotec kits (Catalog #130–100–825 and #130–098–373). Briefly, hearts from 0- to 2-day old mice were excised, chopped into small pieces, and digested using reagents supplied by the kit. A cardiomyocyte-rich cell suspension was obtained by the separation of magnetically labeled non-cardiac cells from the total cell suspension upon application of a magnetic field. $1X10^6$ NMVMs were plated on fibronectin-coated (10 μg/ml) 35 mm (D = 20 mm) glass coverslip dishes (NEST catalog # 801001) in Medium-199 supplemented with 25 mM HEPES, 2 μg/ml Vitamin B12, 50U/ml Pen-strep, non-essential 286 Amino acids, and 10% FBS. The next day, the medium was changed to 2% FBS medium. Adenoviruses expressing CRE-Recombinase (to knockout MCU) or adenoviruses with beta-galactosidase (as a control) were transduced into NMVMs. To monitor mitochondrial Ca^{2+}, the cells were also transduced with adenoviruses expressing the mitochondrially targeted ratiometric Ca^{2+} sensor 4mtd3cpv (74). Cells were transduced at a concentration of ~40 infectious particles per cell on the first or second

day of isolation. IR experiments and imaging were performed on the fifth to sixth day of culture.

Western blot

MCU knockout was confirmed by Western blot (MCU antibody from Cell Signaling #14997), and densitometry analysis using NMVM cell lysates 5 to 6 days after Ad-Cre transduction (Fig. 1).

Inducing IR, $\Delta\Psi_m$, and Ca^{2+} imaging

To monitor mitochondrial membrane potential ($\Delta\Psi_m$), 50 nM Tetramethyl rhodamine methylester (TMRM) was loaded for 30 min at 37 °C prior to the start of the experiment and replaced with fresh modified Tyrode's buffer (130 mM NaCl, 5 mM KCl, 1 mM $MgCl_2$, 10 mM NaHEPES, 1 mM $CaCl_2$ and 5 mM Glucose). A typical protocol included a baseline reading for 10 min followed by 60 min of regional ischemia induced by placing a 15 mm glass coverslip, followed by 60 min of reperfusion upon removal of the coverslip (previously described in NRVMs (25, 75, 76)). During this 130-min period, images were obtained every 15 s on a laser-scanning confocal microscope (Olympus FLUOVIEW 3000RS), where both mitochondrial membrane potential and mitochondrial Ca^{2+} were monitored sequentially at 40X magnification using a silicone-immersion objective (Olympus UPLSAPO40XS). A neutral density filter of 10% was applied to the excitation beam, and cells were imaged with Galvano scanning mode without any averaging. Laser powers of 0.06% for TMRM and 2% for CFP/YFP FRET were used (Fig. 1, *A* and *B*)

Monitoring mitochondrial membrane potential

The excitation wavelength used for TMRM was 561 nm and the emitted fluorescence between 570 and 620 nm was collected. Images were collected every 15 s. When mitochondria are depolarized, TMRM disperses into the cytoplasm from the mitochondria, causing a more diffuse distribution of TMRM fluorescence in the cell. Therefore, we use the spatial dispersion of the signal as an indicator of mitochondrial polarization (77). This is a dimensionless value determined by calculating the coefficient of variation of the image fluorescence intensity (ratio of standard deviation to the mean). This measure minimizes potential artifacts related to bleaching, changes in dye load, and illumination (25, 78).

Monitoring mitochondrial Ca^{2+} and calibration of the probe

Mitochondrial Ca^{2+} was monitored using a genetically encoded FRET probe, 4mtd3cpv. Originally developed by Palmer and Tsien (74), this probe has been characterized for use in cardiac myocytes by Wüst *et. al* (79). It contains four mitochondrial targeting sequences and a circularly permuted Venus group which makes it less susceptible to changes in pH (since pH changes are often seen during Ischemia/Reperfusion). We incorporated this probe into an adenovirus using Invitrogen's Gateway system. Excitation at 445 nm was used to excite CFP, and emissions at 480 nm and 560 nm were collected for ratiometric measurement of mitochondrial Ca^{2+}.

Cytosolic Ca^{2+} measurements

NMVMs were loaded with 2 μM Fura-2AM (Thermo Fisher #F1221) for 30 min at 37 °C before replacing with Tyrode's solution. Ca^{2+} transients were recorded using an inverted fluorescence microscope (Nikon, TE2000), and IonOptix (Myocam) software.

Cytosolic Ca^{2+} was monitored during coverslip-induced I/R using genetically encoded FRET-probe, d3cpv (74). We incorporated this probe into an adenovirus using Invitrogen's Gateway system. NMVMs were transduced on the second day of isolation. Excitation at 445 nm was used to excite CFP, and emissions at 480 nm (for CFP) and 560 nm (for YFP-FRET) were collected for ratiometric measurement of cytosolic Ca^{2+}.

Image analysis

Image series of the time course of the I/R experiment were analyzed using Fiji (https://imagej.net/Fiji/Downloads) (80). A custom-built segmentation-analysis macro was generated to track each cell's $\Delta\Psi_m$ and mCa^{2+} during the in-vitro I/R injury protocol. For mCa^{2+}, the ratio of YFP to CFP was obtained per cell using the "Ratio-Profiler" plugin on Fiji.

Depolarization time estimation

TMRM signal from each cell was subjected to Multi-resolution wavelet decomposition to separate higher frequencies (noise) from large transitions in signal ($\Delta\Psi_m$ depolarizations). Decomposed signals were used to find "transition points" using MATLAB's 'findchangepoints' function.

Oscillation analysis

We generated a FIJI-MATLAB-based Image analysis routine called "MitoWave" (35). Briefly, to obtain the frequency of the oscillating clusters of mitochondria during reperfusion, each cell was separated by segmentation and a difference stack was generated (a stack of image differentials assembled by subtraction of image $i + 1$ from image i). This stack was then summed and segmented to define mitochondrial regions of interest (clusters) showing oscillations of $\Delta\Psi_m$ within the cells. The raw TMRM intensity was then obtained for each mitochondrial cluster. This TMRM signal was subjected to a continuous wavelet transform to obtain a scalogram, using MATLAB's Wavelet Transform toolbox. Each scalogram was then subjected to ImageJ-based thresholding to obtain the coordinates of the major scalogram peaks during reperfusion, thus, the behavior of each oscillating cluster over the duration of reperfusion could be statistically analyzed. Each oscillating cluster was categorized into different frequency bands throughout the reperfusion period. A violin plot visually represents the behavior of these oscillating clusters. Each cluster may change its frequency band during reperfusion, depending on whether it stabilizes or not during reperfusion.

LDH assay

Supernatants were collected from cells subjected to I/R, and a Lactate Dehydrogenase Assay was performed to assess the

level of cellular viability after I/R. CyQUANT LDH Cytotoxicity Assay from Thermo Fisher Scientific was used (Catalog number: C20300). LDH levels were expressed as a percentage of maximum LDH levels released from lysed cells.

Quantification and statistical analysis

Data were analyzed with GraphPad Software (version 8.0) and MATLAB and Statistics Toolbox Release 2019b. Statistical significance between different treatments (genetic knockout or inhibitors) was evaluated with Kruskal-Wallis nonparametric test with Dunn's multiple comparisons test for correction for multiple tests. Summary statistics are presented as mean ± SEM. Statistical analysis for estimating differences in Oscillation patterns was performed with a non-parametric Kolmogorov–Smirnov test using an alpha of 0.001 to reject the null hypothesis. Statistical analysis for estimating significant differences in mCa^{2+} levels with and without CGP-37157 treatment was performed with two-way ANOVA with Dunnett's multiple comparisons test. $p = 0.05$ was used to determine if mCa^{2+} levels were significantly suppressed with CGP-37157 treatment in the middle of Ischemia.

Resource availability

Materials Availability

- The Supplemental Resources Table lists the materials used in this study.
- Mouse lines used in this study were kindly provided through a Uniform Biological Material Transfer Agreement from the laboratory of Dr John Elrod, Temple University, Philadelphia and Dr Elizabeth Murphy, NIH, Bethesda.
- The MitoCam (4mtd3cpv) adenoviral construct provided by Dr Ger Stienen through the Core Facility in the Cardiovascular center, University of Illinois, Chicago.
- This study did not generate new unique reagents.

Data and code availability

Data are contained within the manuscript. Custom macros and MATLAB codes were generated to analyze mitochondrial oscillations. All original code has been deposited at Github (https://github.com/dashok1/MitoWave/tree/v1.0.2) and is publicly available as of the date of publication (35). DOIs are listed in the Table S1.

Supporting information—This article contains supporting information (Supplement Figs. S1-S10, Supplement Videos S1-S9 and Supplemental table S1).

Acknowledgments—We are grateful for the generous contributions of genetically-engineered mice from colonies maintained in the laboratories of Dr John Elrod (MCU Floxed mice) and Dr Elizabeth Murphy (ppif−/− mice).

Author contributions—D. A., B. R., S. S. conceptualization; D. A., K. P., A. S., M. W., T. L., B. R. methodology; D. A., software, formal analysis; D. A., K. P., A. S., M. W., T. L. investigation; D. A. visualization; D. A., B. R. writing - original draft, funding acquisition; B. R. writing - original draft, supervision, resources.

Funding and additional information—This work was supported by National Institutes of Health grants R01HL137259, R01HL134821, S10OD025244 (B. O'R), F31HL134198 and T32HL007227 (D. A.). K. N. P acknowledges support from K12HL141952, AHA CDA 935823 and AHAx PDF 15POST24700006.

Conflict of interests—The authors declare no conflict of interest with the contents of this article.

Abbreviations—The abbreviations used are: ECDF, Empirical Cumulative Distribution; GSHee, reduced Glutathione; I/R, ischemia–reperfusion; LDH, Lactate Dehydrogenase; mCa2+, Mitochondrial Ca2+; mPTP, mitochondrial permeability transition pore; MCU, mitochondrial calcium uniporter; NMVMs, neonatal mouse ventricular myocytes; RIRR, ROS-induced ROS release; ROS, reactive oxygen species.

References

1. Denton, R. M. (2009) Regulation of mitochondrial dehydrogenases by calcium ions. *Biochim. Biophys. Acta* **1787**, 1309–1316
2. Balaban, R. S. (2009) The role of Ca(2+) signaling in the coordination of mitochondrial ATP production with cardiac work. *Biochim. Biophys. Acta* **1787**, 1334–1341
3. Vygodina, T., Kirichenko, A., and Konstantinov, A. A. (2013) Direct regulation of cytochrome c oxidase by calcium ions. *PLoS One* **8**, e74436
4. Murphy, E., and Steenbergen, C. (2008) Ion transport and energetics during cell death and protection. *Physiology (Bethesda)* **23**, 115–123
5. Kirichok, Y., Krapivinsky, G., and Clapham, D. E. (2004) The mitochondrial calcium uniporter is a highly selective ion channel. *Nature* **427**, 360–364
6. Baughman, J. M., Perocchi, F., Girgis, H. S., Plovanich, M., Belcher-Timme, C. A., Sancak, Y., *et al.* (2011) Integrative genomics identifies MCU as an essential component of the mitochondrial calcium uniporter. *Nature* **476**, 341–345
7. De Stefani, D., Raffaello, A., Teardo, E., Szabò, I., and Rizzuto, R. (2011) A 40 kDa protein of the inner membrane is the mitochondrial calcium uniporter. *Nature* **476**, 336–340
8. Chaudhuri, D., Sancak, Y., Mootha, V. K., and Clapham, D. E. (2013) MCU encodes the pore conducting mitochondrial calcium currents. *eLife* **2**, e00704
9. Finkel, T., Menazza, S., Holmström, K. M., Parks, R. J., Liu, J., Sun, J., *et al.* (2015) The ins and outs of mitochondrial calcium. *Circ. Res.* **116**, 1810–1819
10. Pan, X., Liu, J., Nguyen, T., Liu, C., Sun, J., Teng, Y., *et al.* (2013) The physiological role of mitochondrial calcium revealed by mice lacking the mitochondrial calcium uniporter. *Nat. Cell Biol.* **15**, 1464–1472
11. Rasmussen, T. P., Wu, Y., Joiner, M. A., Koval, O. M., Wilson, N. R., Luczak, E. D., *et al.* (2015) Inhibition of MCU forces extramitochondrial adaptations governing physiological and pathological stress responses in heart. *Proc. Natl. Acad. Sci. U. S. A.* **112**, 9129–9134
12. Luongo, T. S., Lambert, J. P., Yuan, A., Zhang, X., Gross, P., Song, J., *et al.* (2015) The mitochondrial calcium uniporter matches energetic supply with cardiac workload during stress and modulates permeability transition. *Cell Rep.* **12**, 23–34
13. Kwong, J. Q., Lu, X., Correll, R. N., Schwanekamp, J. A., Vagnozzi, R. J., Sargent, M. A., *et al.* (2015) The mitochondrial calcium uniporter selectively matches metabolic output to acute contractile stress in the heart. *Cell Rep.* **12**, 15–22
14. Lambert, J. P., Luongo, T. S., Tomar, D., Jadiya, P., Gao, E., Zhang, X., *et al.* (2019) MCUB regulates the molecular composition of the

mitochondrial calcium uniporter channel to limit mitochondrial calcium overload during stress. *Circulation* **140**, 1720–1733
15. Parks, R. J., Menazza, S., Holmström, K. M., Amanakis, G., Fergusson, M., Ma, H., *et al.* (2019) Cyclophilin D-mediated regulation of the permeability transition pore is altered in mice lacking the mitochondrial calcium uniporter. *Cardiovasc. Res.* **115**, 385–394
16. Griffiths, E. J., Ocampo, C. J., Savage, J. S., Rutter, G. A., Hansford, R. G., Stern, M. D., *et al.* (1998) Mitochondrial calcium transporting pathways during hypoxia and reoxygenation in single rat cardiomyocytes. *Cardiovasc. Res.* **39**, 423–433
17. Zorov, D. B., Juhaszova, M., and Sollott, S. J. (2006) Mitochondrial ROS-induced ROS release: an update and review. *Biochim. Biophys. Acta* **1757**, 509–517
18. Aon, M. A., Cortassa, S., Marbán, E., and O'Rourke, B. (2003) Synchronized whole cell oscillations in mitochondrial metabolism triggered by a local release of reactive oxygen species in cardiac myocytes. *J. Biol. Chem.* **278**, 44735–44744
19. Romashko, D. N., Marban, E., and O'Rourke, B. (1998) Subcellular metabolic transients and mitochondrial redox waves in heart cells. *Proc. Natl. Acad. Sci. U. S. A.* **95**, 1618–1623
20. Aon, M. A., Cortassa, S., Maack, C., and O'Rourke, B. (2007) Sequential opening of mitochondrial ion channels as a function of glutathione redox thiol status. *J. Biol. Chem.* **282**, 21889–21900
21. Gong, G., Liu, X., Zhang, H., Sheu, S.-S., and Wang, W. (2015) Mitochondrial flash as a novel biomarker of mitochondrial respiration in the heart. *Am. J. Physiol. Heart Circ. Physiol.* **309**, H1166–H1177
22. Breckwoldt, M. O., Armoundas, A. A., Aon, M. A., Bendszus, M., O'Rourke, B., Schwarzländer, M., *et al.* (2016) Mitochondrial redox and pH signaling occurs in axonal and synaptic organelle clusters. *Sci. Rep.* **6**, 23251
23. Akar, F. G., Aon, M. A., Tomaselli, G. F., and O'Rourke, B. (2005) The mitochondrial origin of postischemic arrhythmias. *J. Clin. Invest.* **115**, 3527–3535
24. Brown, D., and O'Rourke, B. (2010) Cardiac mitochondria and arrhythmias. *Cardiovasc. Res.* **88**, 241–249
25. Solhjoo, S., and O'Rourke, B. (2015) Mitochondrial instability during regional ischemia–reperfusion underlies arrhythmias in monolayers of cardiomyocytes. *J. Mol. Cell Cardiol.* **78**, 90–99
26. Ponnalagu, D., and Singh, H. (2017) Anion channels of mitochondria. *Handb Exp. Pharmacol.* **240**, 71–101
27. Šileikytė, J., Blachly-Dyson, E., Sewell, R., Carpi, A., Menabò, R., Di Lisa, F., *et al.* (2014) Regulation of the mitochondrial permeability transition pore by the outer membrane does not involve the peripheral benzodiazepine receptor (Translocator Protein of 18 kDa (TSPO)). *J. Biol. Chem.* **289**, 13769–13781
28. Seidlmayer, L. K., Hanson, B. J., Thai, P. N., Schaefer, S., Bers, D. M., and Dedkova, E. N. (2021) PK11195 protects from cell death only when applied during reperfusion: succinate-mediated mechanism of action. *Front. Physiol.* **12**, 628508
29. Gunter, T. E., and Pfeiffer, D. R. (1990) Mechanisms by which mitochondria transport calcium. *Am. J. Physiol. Cell Physiol.* **258**, C755–C786
30. Fieni, F., Bae Lee, S., Jan, Y. N., and Kirichok, Y. (2012) Activity of the mitochondrial calcium uniporter varies greatly between tissues. *Nat. Commun.* **3**, 1–12
31. Kwong, J. Q., Huo, J., Bround, M. J., Boyer, J. G., Schwanekamp, J. A., Ghazal, N., *et al.* (2018) The mitochondrial calcium uniporter underlies metabolic fuel preference in skeletal muscle. *JCI Insight* **3**, e121689
32. Hobai, I. A., and O'Rourke, B. (2000) Enhanced Ca^{2+}-activated Na^{+}-Ca^{2+} exchange activity in canine pacing-induced heart failure. *Circ. Res.* **87**, 690–698
33. Drago, I., De Stefani, D., Rizzuto, R., and Pozzan, T. (2012) Mitochondrial Ca2+ uptake contributes to buffering cytoplasmic Ca2+ peaks in cardiomyocytes. *Proc. Natl. Acad. Sci. U. S. A.* **109**, 12986–12991
34. Halestrap, A. P., Clarke, S. J., and Javadov, S. A. (2004) Mitochondrial permeability transition pore opening during myocardial reperfusion—a target for cardioprotection. *Cardiovasc. Res.* **61**, 372–385
35. Ashok, D., and O'Rourke, B. (2021) MitoWave: spatiotemporal analysis of mitochondrial membrane potential fluctuations during I/R. *Biophys. J.* **120**, 3261–3271
36. Zhang, H., Gong, G., Wang, P., Zhang, Z., Kolwicz, S. C., Rabinovitch, P. S., *et al.* (2018) Heart specific knockout of Ndufs4 ameliorates ischemia reperfusion injury. *J. Mol. Cell Cardiol.* **123**, 38–45
37. Basso, E., Fante, L., Fowlkes, J., Petronilli, V., Forte, M. A., and Bernardi, P. (2005) Properties of the permeability transition pore in mitochondria devoid of cyclophilin D. *J. Biol. Chem.* **280**, 18558–18561
38. Hausenloy, D. J., Duchen, M. R., and Yellon, D. M. (2003) Inhibiting mitochondrial permeability transition pore opening at reperfusion protects against ischaemia–reperfusion injury. *Cardiovasc. Res.* **60**, 617–625
39. Ong, S.-B., Samangouei, P., Kalkhoran, S. B., and Hausenloy, D. J. (2015) The mitochondrial permeability transition pore and its role in myocardial ischemia reperfusion injury. *J. Mol. Cell Cardiol.* **78**, 23–34
40. Hunter, D. R., and Haworth, R. A. (1979) The Ca2+ induced membrane transition in mitochondria. *Arch. Biochem. Biophys.* **195**, 453–459
41. Halestrap, A. P., and Richardson, A. P. (2015) The mitochondrial permeability transition: a current perspective on its identity and role in ischaemia/reperfusion injury. *J. Mol. Cell Cardiol.* **78**, 129–141
42. Bernardi, P., and von Stockum, S. (2012) The permeability transition pore as a Ca2+ release channel: new answers to an old question. *Cell Calcium* **52**, 22–27
43. de J García-Rivas, G., Carvajal, K., Correa, F., and Zazueta, C. (2006) Ru360, a specific mitochondrial calcium uptake inhibitor, improves cardiac post-ischaemic functional recovery in rats *in vivo*. *Br. J. Pharmacol.* **149**, 829–837
44. Holmström, K. M., Pan, X., Liu, J. C., Menazza, S., Liu, J., Nguyen, T. T., *et al.* (2015) Assessment of cardiac function in mice lacking the mitochondrial calcium uniporter. *J. Mol. Cell Cardiol.* **85**, 178–182
45. Raffaello, A., De Stefani, D., Sabbadin, D., Teardo, E., Merli, G., Picard, A., *et al.* (2013) The mitochondrial calcium uniporter is a multimer that can include a dominant-negative pore-forming subunit. *EMBO J.* **32**, 2362–2376
46. Beutner, G., Sharma, V. K., Lin, L., Ryu, S.-Y., Dirksen, R. T., and Sheu, S.-S. (2005) Type 1 ryanodine receptor in cardiac mitochondria: transducer of excitation–metabolism coupling. *Biochim. Biophys. Acta* **1717**, 1–10
47. Jakob, R., Beutner, G., Sharma, V. K., Duan, Y., Gross, R. A., Hurst, S., *et al.* (2014) Molecular and functional identification of a mitochondrial ryanodine receptor in neurons. *Neurosci. Lett.* **575**, 7–12
48. Jiang, D., Zhao, L., Clish, C. B., and Clapham, D. E. (2013) Letm1, the mitochondrial Ca2+/H+ antiporter, is essential for normal glucose metabolism and alters brain function in Wolf–Hirschhorn syndrome. *Proc. Natl. Acad. Sci. U. S. A.* **110**, E2249–E2254
49. Tsai, M.-F., Jiang, D., Zhao, L., Clapham, D., and Miller, C. (2014) Functional reconstitution of the mitochondrial Ca2+/H+ antiporter Letm1. *J. Gen. Physiol.* **143**, 67–73
50. Griffiths, E. J. (1999) Reversal of mitochondrial Na/Ca exchange during metabolic inhibition in rat cardiomyocytes. *FEBS Lett.* **453**, 400–404
51. Nicholls, D. G., and Crompton, M. (1980) Mitochondrial calcium transport. *FEBS Lett.* **111**, 261–268
52. Drago, I., Pizzo, P., and Pozzan, T. (2011) After half a century mitochondrial calcium in- and efflux machineries reveal themselves. *EMBO J.* **30**, 4119–4125
53. Moreau, B., and Parekh, A. B. (2008) Ca2+-Dependent inactivation of the mitochondrial Ca2+ uniporter involves proton Flux through the ATP synthase. *Curr. Biol.* **18**, 855–859
54. Maack, C., Cortassa, S., Aon, M., Ganesan, A., Liu, T., and O'Rourke, B. (2006) Elevated cytosolic Na+ decreases mitochondrial Ca2+ uptake during excitation-contraction coupling and impairs energetic adaptation in cardiac myocytes. *Circ. Res.* **99**, 172–182
55. Cox, D. A., Conforti, L., Sperelakis, N., and Matlib, M. A. (1993) Selectivity of inhibition of Na+-Ca2+ exchange of heart mitochondria by benzothiazepine CGP-37157. *J. Cardiovasc. Pharmacol.* **21**, 595–599
56. Neumann, J. T., Diaz-Sylvester, P. L., Fleischer, S., and Copello, J. A. (2011) CGP-37157 inhibits the sarcoplasmic reticulum Ca2+ ATPase and activates ryanodine receptor channels in striated muscle. *Mol. Pharmacol.* **79**, 141–147
57. Thu, L. T., Ahn, J. R., and Woo, S.-H. (2006) Inhibition of L-type Ca2+ channel by mitochondrial Na+–Ca2+ exchange inhibitor CGP-37157 in rat atrial myocytes. *Eur. J. Pharmacol.* **552**, 15–19

58. Crompton, M., Künzi, M., and Carafoli, E. (1977) The calcium-induced and sodium-induced effluxes of calcium from heart mitochondria. *Eur. J. Biochem.* **79**, 549–558
59. Wolkowicz, P. E., Michael, L. H., Lewis, R. M., and McMillin-Wood, J. (1983) Sodium-calcium exchange in dog heart mitochondria: effects of ischemia and verapamil. *Am. J. Physiol. Heart Circ. Physiol.* **244**, H644–H651
60. Brand, M. D. (1985) The stoichiometry of the exchange catalysed by the mitochondrial calcium/sodium antiporter. *Biochem. J.* **229**, 161–166
61. Affolter, H., and Carafoli, E. (1980) The Ca2+-Na+ antiporter of heart mitochondria operates electroneutrally. *Biochem. Biophys. Res. Commun.* **95**, 193–196
62. Baysal, K., Jung, D. W., Gunter, K. K., Gunter, T. E., and Brierley, G. P. (1994) Na(+)-dependent Ca2+ efflux mechanism of heart mitochondria is not a passive Ca2+/2Na+ exchanger. *Am. J. Physiol. Cell Physiol.* **266**, C800–C808
63. Jung, D. W., Baysal, K., and Brierley, G. P. (1995) The sodium-calcium antiport of heart mitochondria is not electroneutral. *J. Biol. Chem.* **270**, 672–678
64. Kim, B., and Matsuoka, S. (2008) Cytoplasmic Na+-dependent modulation of mitochondrial Ca2+ *via* electrogenic mitochondrial Na+–Ca2+ exchange. *J. Physiol.* **586**, 1683–1697
65. Paucek, P., and Jabůrek, M. (2004) Kinetics and ion specificity of Na+/Ca2+ exchange mediated by the reconstituted beef heart mitochondrial Na+/Ca2+ antiporter. *Biochim. Biophys. Acta* **1659**, 83–91
66. Wei, A.-C., Liu, T., Cortassa, S., Winslow, R. L., and O'Rourke, B. (2011) Mitochondrial Ca2+ influx and efflux rates in Guinea pig cardiac mitochondria: low and high affinity effects of cyclosporine A. *Biochim. Biophys. Acta* **1813**, 1373–1381
67. Palty, R., Hershfinkel, M., and Sekler, I. (2012) Molecular identity and functional properties of the mitochondrial Na^+/Ca^{2+} exchanger. *J. Biol. Chem.* **287**, 31650–31657
68. Wang, W., Fang, H., Groom, L., Cheng, A., Zhang, W., Liu, J., *et al.* (2008) Superoxide flashes in single mitochondria. *Cell* **134**, 279–290
69. O-Uchi, J., Jhun, B. S., Mishra, J., and Sheu, S.-S. (2018) Organellar ion channels and transporters. In *Cardiac Electrophysiology: From Cell to Bedside*, 7th Ed., Elsevier, Philadelphia, PA: 66–79
70. Cortassa, S., Aon, M. A., Winslow, R. L., and O'Rourke, B. (2004) A mitochondrial oscillator dependent on reactive oxygen species. *Biophys. J.* **87**, 2060–2073
71. Kim, J.-S., Jin, Y., and Lemasters, J. J. (2006) Reactive oxygen species, but not Ca2+ overloading, trigger pH- and mitochondrial permeability transition-dependent death of adult rat myocytes after ischemia-reperfusion. *Am. J. Physiol. Heart Circ. Physiol.* **290**, H2024–H2034
72. Aon, M. A., Cortassa, S., and O'Rourke, B. (2008) Mitochondrial oscillations in physiology and pathophysiology. *Adv. Exp. Med. Biol.* **641**, 98–117
73. Solhjoo, S., Liu, T., Sidor, A., Lee, D. I., O'Rourke, B., and Steenbergen, C. (2023) Oxidative stress in the mitochondrial matrix underlies ischemia/reperfusion-induced mitochondrial instability. *J. Biol. Chem.* **299**, 102780
74. Palmer, A. E., Giacomello, M., Kortemme, T., Hires, S. A., Lev-Ram, V., Baker, D., *et al.* (2006) Ca2+ indicators based on computationally redesigned calmodulin-peptide pairs. *Chem. Biol.* **13**, 521–530
75. Pitts, K. R., and Toombs, C. F. (2004) Coverslip hypoxia: a novel method for studying cardiac myocyte hypoxia and ischemia *in vitro*. *Am. J. Physiol. Heart Circ. Physiol.* **287**, H1801–H1812
76. de Diego, Carlos, Pai Rakesh, K., Chen, Fuhua, Xie, Lai-Hua, De Leeuw, Jan, Weiss James, N., *et al.* (2008) Electrophysiological consequences of acute regional ischemia/reperfusion in neonatal rat ventricular myocyte monolayers. *Circulation* **118**, 2330–2337
77. Lemasters, J. J., and Ramshesh, V. K. (2007) Imaging of mitochondrial polarization and depolarization with cationic fluorophores. In , 2nd Edition,*MitochondriaMethods in Cell Biology* Academic Press, Cambridge, MA: 283–295
78. Duchen, M. R., Surin, A., and Jacobson, J. (2003) Imaging mitochondrial function in intact cells. *Met. Enzymol.* **361**, 353–389
79. Wüst, R. C. I., Helmes, M., Martin, J. L., Wardt, T. J. T. van der, Musters, R. J. P., Velden, J. van der, *et al.* (2017) Rapid frequency-dependent changes in free mitochondrial calcium concentration in rat cardiac myocytes. *J. Physiol.* **595**, 2001–2019
80. Schindelin, J., Arganda-Carreras, I., Frise, E., Kaynig, V., Longair, M., Pietzsch, T., *et al.* (2012) Fiji: an open-source platform for biological-image analysis. *Nat. Met.* **9**, 676–682